On the Numerical Simulation of Metasurfaces With Impedance Boundary Condition Integral Equations

On the Numerical Simulation of Metasurfaces with Impedance Boundary Condition Integral Equations

Matteo Alessandro Francavilla, *Member, IEEE*, Enrica Martini, *Senior Member, IEEE*, Stefano Maci, *Fellow, IEEE*, Giuseppe Vecchi, *Fellow, IEEE*

***Abstract*—Metasurfaces are thin metamaterial layers characterized by unusual dispersion properties of surface/guided wave and/or reflection properties of otherwise incident plane waves. At the scales intervening in their design, metasurfaces can be described through a surface impedance boundary condition. The impedance, possibly tensorial, is often "modulated" i.e. it can vary from place to place on the surface (by design). We investigate on different integral equation formulations of the problem, with special attention to the stability properties of the resulting system matrix.**

***Index Terms*—Metasurfaces, Moment methods (MoM), integral equations, impedance boundary condition (IBC), anisotropic surface impedance.**

I. Introduction

In recent years metamaterials have inspired several applications in designing antennas and microwave components, thanks to the possibility of achieving electromagnetic properties impossible to find in nature. Metasurfaces are thin metamaterial layers characterized by unusual reflection properties of plane waves and/or dispersion properties of surface/guided waves [1], [2]. Metasurfaces can be realized at microwave frequencies by printing a dense periodic texture of small elements on a grounded slab, with or without shorting vias; in the following, we will refer with the term metasurface to the *combination* of grounded slab and printed metalizations on top of it. Because the patterning is sub-wavelength, wave phenomena on the metasurface can be suitably approximated in terms of an equivalent surface impedance relating the tangential components of the average electric and magnetic fields. This surface impedance typically takes on space-dependent values to realize guiding or radiating components [3]–[5]. By modulating the equivalent surface impedance it is possible to engineer the interaction of a given incoming field with the metasurface so as to design a large number of devices [6]. For instance, metasurfaces can be used to change the propagation constant of surface waves, thus realizing planar lenses [7], or leaky-wave antennas [3]–[5]. The very effect of metasurface antennas and lenses derives from the spatial variability of the (tensorial) surface impedance, sought by design.

Manuscript received June XX, 2014. The presented research activity is partly funded by the "Multiscale Modeling of Electronic Materials" CRA CDE3M (B.2).

M. A. Francavilla is with the Antenna and EMC Lab (LACE), Istituto Superiore Mario Boella, Torino 10138, Italy (e-mail: francavilla@ismb.it).

G. Vecchi is with the Antenna and EMC Lab (LACE), Politecnico di Torino, Torino 10128, Italy (e-mail: giuseppe.vecchi@polito.it).

E. Martini and S. Maci are with the Department of Information Engineering, University of Siena, 53100 Siena, Italy (e-mail: martini@dii.unisi.it; macis@dii.unisi.it).

The metasurface modulation can be obtained by gradually changing the geometry of the elements in contiguous cells, while maintaining the period unchanged and very small in terms of a wavelength. Macroscopically, this results in a modulation of the equivalent impedance of the metasurface, that, due to the small dimensions of the unit cell, can be assumed to be almost continuous. Metasurfaces consisting of electrically small printed patches with a symmetric shape result in a surface impedance that is mostly scalar. By using asymmetric constituent elements, however, it is possible to design metasurfaces with specific anisotropic behaviors. This kind of artificial surfaces can be effectively described through an equivalent impedance tensor. It has been recently suggested that modulated anisotropic metasurfaces can be used to re-address the propagation path of an incident surface wave [8]. This approach provides effects similar to those obtained by applying Transformation Optics in volumetric inhomogeneous metamaterials, but with a significant technological simplification.

The typical design of a metasurface device starts from an analytic determination of the surface impedance (e.g. [5], [9]) which rests on some approximation; this surface impedance is then realized by appropriately sized cells, with this design phase usually based on a local periodicity assumption. It is therefore desirable to have an intermediate tool to assist antenna engineers during the design phase: such tool shall be able to predict the electromagnetic behavior of a given surface impedance profile without further approximations; the cell design process can thus start after the surface impedance has proven to produce the desired performances. During all retuning of the metasurface, only the impedance profile needs be updated, with no mesh change necessary, and without the explicit CAD drawing of all cells. This drastically reduces the time needed to optimize sizes, shapes and locations of the single elements. Likewise, the necessary full-wave analysis of the actual structure will be typically carried out only at the end of the design process, with minimal retuning of the individual cells.

Motivated by this, we investigate on the full-wave solution of the boundary-value problem for the IBC in realistic geometries employing the integral-equation formulation (with Method of Moments (MoM) discretization). In particular, we address the stability properties of the associated numerical problem, which play a crucial role in the analysis of the metasurface. Obviously, we are not addressing here the problem of how to design a reactance profile satisfying some goal requirements. However, we hope that our finding will

expedite the design process. Finally, we remark that during design retuning where only the impedance profile is changed, key components of the MoM matrix need not be re-computed (even when using fast factorizations), significantly expediting this optimization phase.

A recent paper [10] has addressed the problem of scattering from IBC surfaces in a very efficient and promising way, by discretizing both electric and magnetic currents and thanks to a self-dual formulation stable with frequency and impedance. However, applying [10] to thin layer problems, as the ones arising from metasurface analysis, is non-trivial. Here, we explore different formulations to analyze the very specific problem of metasurfaces, including how to extend the validity of the IBC itself (i.e. how to better cope with spatial dispersivity).

Finally, it is worth mentioning here that Generalized Sheet Transition Conditions (GSTC) [11], [12] generally provide a more general description of the metasurface; there is a connection between the GSTC and IBC, which is discussed in [2]. Further, we remark here that the aim of this work is not discussing under which conditions the IBC is applicable; on the contrary, we address the numerical issues arising in dealing with the IBC when this is satisfactorily applicable. There is indeed a vast literature discussing the validity of the IBC model (see, e.g., [13] and references therein).

The remainder of the paper is organized as follows: in Section II, we introduce three different integral formulations to address metasurfaces; Section III discusses the stability properties of the formulations, and in Section IV a set of real-life metasurfaces is presented to analyze the performance of these formulations. Preliminary results and applications of the proposed approach have been presented in conference papers [14], [15]. Finally, a brief conclusion is given in Section V.

II. Formulation

With reference to Fig. 1, the (tensor) surface Impedance Boundary Condition (IBC) on a surface Σ can be written in two ways:

a) relating the rotated tangential traces of the fields on the exterior of a closed surface (or half-space) [10], [16]–[20]

$$\hat{\mathbf{n}} \times \mathbf{E}_{\Sigma^+} = \hat{\mathbf{n}} \times \left[\underline{\underline{Z}}_s \cdot (\hat{\mathbf{n}} \times \mathbf{H}_{\Sigma^+}) \right] \tag{1}$$

where $\hat{\mathbf{n}}$ is the (outward) unit vector normal to the surface Σ, $\underline{\underline{Z}}_s$ is the tensorial surface impedance, and the subscripts Σ^+ and Σ^- indicate whether the field is evaluated in the limit approaching Σ from the direction identified by $\hat{\mathbf{n}}$ or $-\hat{\mathbf{n}}$, respectively; or

b) relating the rotated tangential trace of the average electric field to the rotated tangential trace of the magnetic field jump across an infinitely thin surface [2], [12]

$$\hat{\mathbf{n}} \times \mathbf{E}_{av} = \hat{\mathbf{n}} \times \left[\underline{\underline{Z}}_s \cdot \Big(\hat{\mathbf{n}} \times (\mathbf{H}_{\Sigma^+} - \mathbf{H}_{\Sigma^-}) \Big) \right] \tag{2}$$

Equations (1) and (2) are sometimes denoted as *zeroth order* IBCs [13], and the impedance parameters are valid only for single incidence (typically, normal incidence for scattering, and surface wave incidence for metasurface antennas); higher order IBCs provide a more accurate modeling of the impedance surface, at the additional cost of being non local. In the following, we will not discuss higher order IBCs, as the subject goes beyond the scope of the paper; rather, we will focus our attention on the numerical stability of the zeroth order IBCs, specifically in the presence of a reactive impedance boundary condition, extending its validity beyond the single incidence.

Our aim is to solve (1) or (2) by means of the Method of Moments (MoM). We start by expressing the electric and magnetic fields as a function of the tangential components of the fields on the equivalent surface $\Sigma = \Sigma^+ \cup \Sigma^-$, a closed boundary enclosing the metasurface (shown in fig. 1), in virtue of the uniqueness and Love theorems. To this aim we resort to Stratton-Chu formulation [21] for the scattered fields:

$$\begin{aligned} \mathbf{E}^s = &\int_\Sigma \underline{\underline{\mathcal{G}}}^{ej}(\mathbf{r},\mathbf{r}') \cdot \big(\hat{\mathbf{n}}_\Sigma \times \mathbf{H}_\Sigma(\mathbf{r}')\big)\, d\mathbf{r}' + \\ &\int_\Sigma \underline{\underline{\mathcal{G}}}^{em}(\mathbf{r},\mathbf{r}') \cdot \big(-\hat{\mathbf{n}}_\Sigma \times \mathbf{E}_\Sigma(\mathbf{r}')\big)\, d\mathbf{r}' \\ \mathbf{H}^s = &\int_\Sigma \underline{\underline{\mathcal{G}}}^{hj}(\mathbf{r},\mathbf{r}') \cdot \big(\hat{\mathbf{n}}_\Sigma \times \mathbf{H}_\Sigma(\mathbf{r}')\big)\, d\mathbf{r}' + \\ &\int_\Sigma \underline{\underline{\mathcal{G}}}^{hm}(\mathbf{r},\mathbf{r}') \cdot \big(-\hat{\mathbf{n}}_\Sigma \times \mathbf{E}_\Sigma(\mathbf{r}')\big)\, d\mathbf{r}' \end{aligned} \tag{3}$$

where $\underline{\underline{\mathcal{G}}}^{ej}$, $\underline{\underline{\mathcal{G}}}^{em}$, $\underline{\underline{\mathcal{G}}}^{hj}$ and $\underline{\underline{\mathcal{G}}}^{hm}$ are suitable (i.e. problem dependant) dyadic Green's functions.

A. Opaque IBC-EFIE

Let's consider the *opaque* or *one-sided* IBC of eq. (1): this model assumes that the impedance sheet is impenetrable, which in turn implies that fields on the negative side Σ^- are null, and substitution of (3) into (1) yields:

$$\begin{aligned} &\hat{\mathbf{n}} \times \mathbf{E}^{inc}_{\Sigma^+} + \hat{\mathbf{n}} \times \int_\Sigma \underline{\underline{\mathcal{G}}}^{ej} \cdot \big(\hat{\mathbf{n}} \times \mathbf{H}_{\Sigma^+}\big)\, d\mathbf{r}' + \\ &\hat{\mathbf{n}} \times \int_\Sigma \underline{\underline{\mathcal{G}}}^{em} \cdot \big(-\hat{\mathbf{n}} \times \mathbf{E}_{\Sigma^+}\big)\, d\mathbf{r}' = \hat{\mathbf{n}} \times \left[\underline{\underline{Z}}_s \cdot (\hat{\mathbf{n}} \times \mathbf{H}_{\Sigma^+}) \right] \end{aligned} \tag{4}$$

with $\hat{\mathbf{n}} \equiv \hat{\mathbf{n}}_{\Sigma^+}$. In the opaque model, the tensor $\underline{\underline{Z}}_s$ accounts for the sheet impedance (e.g., the patches) and the grounded dielectric slab; consequently, the sheet currents $\mathbf{J} = \hat{\mathbf{n}} \times \mathbf{H}_{\Sigma^+}$ and $\mathbf{M} = -\hat{\mathbf{n}} \times \mathbf{E}_{\Sigma^+} = -\hat{\mathbf{n}} \times \big(\underline{\underline{Z}}_s \cdot \mathbf{J} \big)$ radiate in free space, and the appropriate Green's functions are:

$$\underline{\underline{\mathcal{G}}}^{ej}(\mathbf{r},\mathbf{r}') = jk \left[\underline{\underline{I}} + \frac{\nabla\nabla'}{k^2} \right] \frac{e^{-jkR}}{4\pi R}$$

$$\underline{\underline{\mathcal{G}}}^{em}(\mathbf{r},\mathbf{r}') = \nabla \times \left(\frac{e^{-jkR}}{4\pi R} \underline{\underline{I}} \right)$$

with $R = \|\mathbf{r} - \mathbf{r}'\|$, and $k = \omega\sqrt{\varepsilon_0 \mu_0}$. Note that, when the surface Σ^+ is planar, the principal value of $\hat{\mathbf{n}} \times \int_\Sigma \underline{\underline{\mathcal{G}}}^{em} \cdot \mathbf{M}\, d\mathbf{r}'$ vanishes, and the integral reduces to $-1/2\mathbf{M}$. This assumption is always valid for the planar metasurfaces considered here, and substitution of eq. (1) into eq. (4) yields the following modified Electric Field Integral Equation (EFIE):

$$\hat{\mathbf{n}} \times \mathbf{E}^{inc} = -\hat{\mathbf{n}} \times \int_\Sigma \underline{\underline{\mathcal{G}}}^{ej} \cdot \mathbf{J}\, d\mathbf{r}' + \frac{1}{2} \hat{\mathbf{n}} \times \big(\underline{\underline{Z}}_s \cdot \mathbf{J} \big) \tag{5}$$

Eq. (5) is an equation in one unknown (the *equivalent* electric current density $\mathbf{J} = \hat{\mathbf{n}} \times \mathbf{H}_{\Sigma^+}$), which can be discretized and solved by means of the MoM.

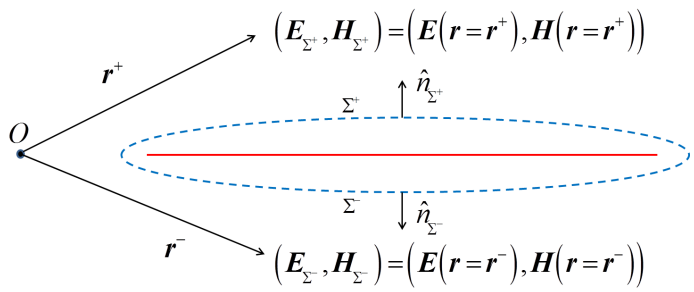

Fig. 1. The geometry for deriving the integral equation describing the metasurface (identified in red).

B. Transparent IBC-EFIE

Conversely, if one aims to solve eq. (2), after expressing the left hand side as $\hat{\mathbf{n}}\times\mathbf{E}_{av}=\frac{1}{2}\hat{\mathbf{n}}\times\left(\mathbf{E}_{\Sigma+}+\mathbf{E}_{\Sigma-}\right)$, analogous derivations and the introduction of the two equivalent current densities $\mathbf{J}=\hat{\mathbf{n}}\times(\mathbf{H}_{\Sigma+}-\mathbf{H}_{\Sigma-})$ and $\mathbf{M}=-\hat{\mathbf{n}}\times(\mathbf{E}_{\Sigma+}-\mathbf{E}_{\Sigma-})$ yield:

$$\begin{aligned}\hat{\mathbf{n}}\times\mathbf{E}^{inc}=&-\hat{\mathbf{n}}\times\int_{\Sigma}\underline{\underline{\mathcal{G}}}^{ej}\cdot\mathbf{J}\,d\mathbf{r}'-\\&\hat{\mathbf{n}}\times\int_{\Sigma}\underline{\underline{\mathcal{G}}}^{em}\cdot\mathbf{M}\,d\mathbf{r}'+\hat{\mathbf{n}}\times\left(\underline{\underline{Z}}_s\cdot\mathbf{J}\right)\end{aligned}\tag{6}$$

Differently from the opaque case, $\underline{\underline{Z}}_s$ now does not take into account the grounded slab, as it only describes the field jump across the sheet of patches. The effect of the slab, on the other hand, has to be accounted for by the Green's functions. Several formulations are well known in literature for modeling the Green's functions in layered media; a discussion about them goes beyond the scope of the present paper, and we will only mention that the formulation employed in the remainder of the paper is the Mixed-Potential formulation by Michalski [22]. Obviously, once the characteristics of the grounded dielectric slab are chosen (i.e., its thickness h and its permittivity/permeability), there is a one-to-one relation [23] between the two impedance tensors of eq. (1) and (2), which is particularly simple when a TE/TM basis is fixed:

$$\underline{\underline{Y}}_s^{opaque}=\underline{\underline{Y}}_s^{transp}+\begin{bmatrix}Y_{slab}^{TM}(k_s)&0\\0&Y_{slab}^{TE}(k_s)\end{bmatrix}\tag{7}$$

where $\underline{\underline{Y}}_s=\underline{\underline{Z}}_s^{-1}$, and the admittances of the slab Y_{slab}^{TM} and Y_{slab}^{TE} explicitely depend on the (local) wavenumber k_s of the guided wave:

$$\begin{aligned}Y_{slab}^{TM}&=-j\frac{\omega\varepsilon}{k_z}\cot(k_zh)\\Y_{slab}^{TE}&=-j\frac{k_z}{\omega\mu}\cot(k_zh)\end{aligned}\tag{8}$$

where $k_z=\sqrt{k^2-k_s^2}$. Note that, for normal incidence, $\frac{\omega\varepsilon}{k_z}=\frac{k_z}{\omega\mu}=\sqrt{\frac{\varepsilon}{\mu}}$, and $Y_{slab}^{TM}=Y_{slab}^{TE}$, as expected (the two polarizations are indistinguishable). It is worth noting here that k_s in eq. (7) is the transverse wavenumber of the surface wave locally supported by the structure, and it is obtained by solving the local resonance equation [6].

Eq. (6) is an equation in two unknowns ($\mathbf{J}$ and $\mathbf{M}$), and requires an additional condition to be enforced, e.g. the dual of eq. (2), relating the average magnetic field to the jump of the electric field:

$$\hat{\mathbf{n}}\times\mathbf{H}_{av}=\hat{\mathbf{n}}\times\left[\underline{\underline{Y}}_{ms}\cdot\left(-\hat{\mathbf{n}}\times(\mathbf{E}_{\Sigma+}-\mathbf{E}_{\Sigma-})\right)\right]\tag{9}$$

Note that the surface *magnetic* admittance $\underline{\underline{Y}}_{ms}$ is a tensor independent from $\underline{\underline{Z}}_s$ (see [2] and references therein). However, under the assumption that the patches synthesizing the metasurfaces are thin, the tangential electric field is continuous (null on metalizations, continuous across a dielectric interface), yielding $\mathbf{M}=\hat{\mathbf{n}}\times(\mathbf{E}_{\Sigma+}-\mathbf{E}_{\Sigma-})=0$. In the following we will restrict our attention to the case where this assumption is valid, so that the term $\int_\Sigma\underline{\underline{\mathcal{G}}}^{em}\cdot\mathbf{M}\,d\mathbf{r}'$ does not contribute to radiation, and eq. (6) can be solved for the sole unknown $\mathbf{J}$.

It is worth mentioning here that the formulation of eq. (6) is general, and is not limited to planarly layered media; however, in the presence of different backgrounds, Green's functions are available only in a few cases (e.g., in the case of coated cylinders [24]). On the other hand, when the Green's function of the problem is not available, the numerical solution of eq. (2) requires discretization of the interfaces between different media (see, e.g., [10], [17]). In the rest of the paper, without loss of generality, we will focus on planar stratifications only.

C. Alternative IBC-EFIE

A slightly different formulation to discretize eq. (1) is also possible: with reference to Fig. 2, the equivalence surface is built to enclose the dielectric slab, with its boundary represented by the metasurface (Σ^+ in figure), the metallic ground plane (Σ^-), and the closure where the slab is truncated (Σ^e). For thin substrates it is typically reasonable to neglect the effects of the currents on sidewalls Σ^e, and the following equations can then be derived:

$$\begin{aligned}\hat{\mathbf{n}}_{\Sigma^+}\times\mathbf{E}_{\Sigma^+}=\hat{\mathbf{n}}_{\Sigma^+}\times\left[\underline{\underline{Z}}_s\cdot(\hat{\mathbf{n}}_{\Sigma^+}\times\mathbf{H}_{\Sigma^+})\right]\ \text{on}\ \Sigma^+\\\hat{\mathbf{n}}_{\Sigma^-}\times\mathbf{E}_{\Sigma^-}=0\ \text{on}\ \Sigma^-\end{aligned}\tag{10}$$

These boundary conditions require the presence of electric currents $\mathbf{J}^-=\hat{\mathbf{n}}_{\Sigma^-}\times\mathbf{H}_{\Sigma^-}$ on Σ^-, and electric and magnetic currents, $\mathbf{J}^+=\hat{\mathbf{n}}_{\Sigma^+}\times\mathbf{H}_{\Sigma^+}$ and $\mathbf{M}^+=-\hat{\mathbf{n}}_{\Sigma^+}\times\mathbf{E}_{\Sigma^+}=-\hat{\mathbf{n}}_{\Sigma^+}\times\left(\underline{\underline{Z}}_s\cdot\mathbf{J}^+\right)$, on Σ^+. As in the case of eq. (5), magnetic currents are expressed in terms of electric currents, and (10) is a system of two equations in two unknowns ($\mathbf{J}^+$ and $\mathbf{J}^-$). Love's equivalence theorem applied on $\Sigma^+\cup\Sigma^-$ allows to remove the dielectric slab and fill the interior volume with free space; consequently, $\mathbf{J}^+$ and $\mathbf{J}^-$ radiate in a homogeneous medium, with the same Green's functions as in eq. (5).

III. Stability of the Formulations

A. Condition properties of the IBC-EFIE formulations

In order to focus on the relevant properties of the formulations, tests have first been carried out with the smallest meaningful size; we considered a square patch of size 0.1λ (the frequency of analysis is $f_0=7.5$GHz), discretized with 4 triangles and analyzed by means of a MoM discretization with Rao-Wilton-Glisson (RWG) [25] basis functions and tested onto $\hat{n}\times$RWG. The surface impedance is constant and

isotropic, i.e., $\underline{\underline{Z}}_s = Z_s \underline{\underline{I}}$, with $\underline{\underline{I}}$ the identity dyad. The condition number of the MoM matrix is studied as a function of the impedance value Z_s; Fig. 3(a) summarizes the behavior of the condition number, when the real and imaginary components of the surface impedance Z_s vary in the interval $[-10Z_0, 10Z_0]$, with $Z_0 = \sqrt{\frac{\mu_0}{\varepsilon_0}}$ the wave impedance in vacuum; three distinct peaks of the condition number are clearly visible on the imaginary axis of Z_s. When increasing the discretization, the number of peaks in the condition number increases too (see fig. 4(a), referring to a square plate discretized with 313 unknowns); eventually, for very dense discretizations, the problem is ill-posed in a continuous interval on the positive imaginary axis. By looking at the spectrum of the discretized operator for the problem with 4 unknowns (fig. 3(b)), it is clear that some imaginary impedance values have the effect of moving one singular value of the system matrix to the origin, accordingly making the system ill conditioned. Note that typical values of reactance required to support surface waves in a metasurface fall into the ill-conditioned interval. We stress that the above analysis is merely a study of the numerical properties of the discretization of the IBC equations; consequently, some values of Z_s in the considered range may not correspond to realistic structures (e.g., $R_s < 0$). It is worth noting that the problem is intrinsically linked to the specific reactance values implied by metasurfaces, which are in turn solutions of a transverse resonance problem (see, e.g., [8] and references therein); conversely, it does not show up when studying the scattering from a surface described through reactive IBCs (e.g., successfully analyzed with the one-sided IBC-EFIE in [26]), nor for real values of the surface impedance $Z_s \in \mathbb{R}$ [16], [17], [27].

Conversely, different properties of the IBC-EFIE are obtained when eq. (6) is enforced. Despite the equation has still the same form of the one-sided IBC-EFIE in (5), and as a consequence instability regions for some values of Z_s are expected, it can be verified that the region where the transparent IBC-EFIE is unstable is different from the region where the one-sided IBC-EFIE is unstable, as shown in fig. 4(b), where the condition number of the IBC-EFIE is studied as a function of the normalized reactance $\frac{X_s}{Z_0}$. The results show how the instability region is shifted; most important, typical values of X_s involved in metasurfaces lie in the instability range of the one-sided IBC-EFIE, but not in the instability range of the transparent IBC-EFIE.

Consequently, the transparent IBC has a twofold benefit over the opaque IBC:

- it yields a well-conditioned matrix equation for typical metasurface reactances, as shown in fig. 4(b).
- the spatial dispersion in the dielectric slab is taken into account by the layered Green's functions (and, therefore, the slab admittance Y_{slab}^{TM} extracted in (7) depends explicitly on k_s); this is not true for the case of the one-sided IBC, where the spatial dispersion is neglected, which is both incorrect and unphysical. Note that the dispersion of the impedance sheets (typically realized with sub-wavelength metallic patches) is always neglected; however, it can be verified that the dispersion of the patches is typically negligible. The importance of spatial dispersion and its effects on metasurface problems have been discussed in two recent works [28], [29].

We observe that this formulation, while different, is in agreement with the recommendations of [2] on the descriptors of the IBC.

B. Isotropic surface impedance: planar Luneburg lens

We next consider the case of an impedance profile corresponding to the Luneburg lens:

$$Z_s = jZ_0\sqrt{\frac{k_s^2}{k^2}\left[2-\left(\frac{\rho}{R}\right)^2\right]-1} \qquad (11)$$

where ρ is the distance from the center, $R = 12.5cm$ is the radius of the lens, and k_s is the wavenumber of the TM guided wave supported by the structure (a PEC-backed dielectric slab). The lens has been discretized with 12'510 RWG functions, and analyzed at the frequency of 7.5 GHz. The impedance profile described by (11) possesses the property of focusing parallel rays into a single point on the edge of the lens (or, reciprocally, transforming rays launched by a point source on the edge into a plane wavefront on the opposite side of the lens). If one applies the one-sided IBC (5) to analyze the structure the resulting MoM matrix is very ill-conditioned, and an iterative solution fails to converge (see fig. 5). On the other hand, if one uses the transparent IBC (6) the resulting system matrix is well-conditioned, and the system converges to the correct solution, as in Fig. 6. This option requires explicitly taking into account a specific dielectric slab, and evaluating the Green's functions in a layered medium; Fig. 6 shows the current density on the lens with an Arlon AR 1000 dielectric substrate ($\varepsilon_r = 9.8$, thickness $h = 1.575mm$) and excited through a point source placed in $(x = R, y = 0)$, when eq. (6) is enforced: as expected, the correct focusing behavior of the Luneburg lens is satisfactorily captured. Conversely, when eqs. (5)-(10) are enforced, it is impossible to correctly predict fields on the surface of the lens (see Figs. 7-8).

An explanation of the reason why the opaque IBC-EFIE fails to correctly model the metasurface can be given as follows: when applying eq. (1), one is analyzing a resonant problem (as a matter of fact, the surface reactance X_s is obtained as a solution of a resonant problem). On the other hand, when the problem is modeled by means of eq. (2), one

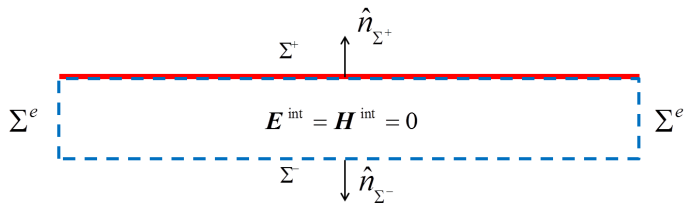

Fig. 2. Alternative application of the equivalence theorem to derive the integral formulation of the IBC on the metasurface (identified in red): the equivalence surface (the blue dashed line in figure) is split into: a) Σ^+, where the one-sided IBC is enforced; b) Σ^-, where the PEC condition is enforced; c) Σ^e, the *lateral* edges of the closed surfaces, which are neglected.

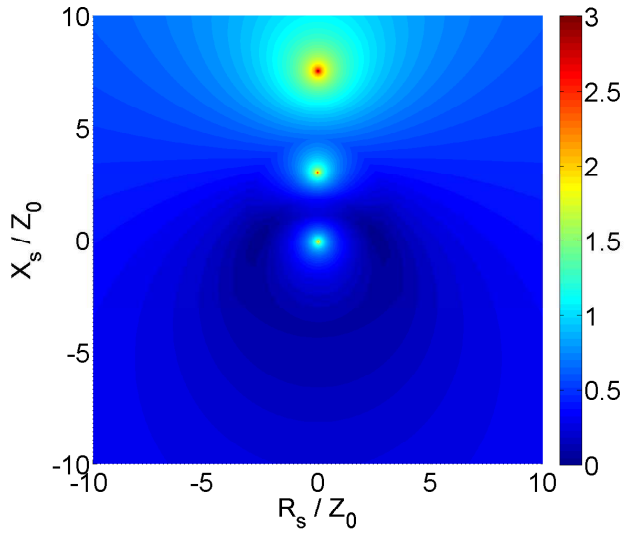

(a) $\log_{10}$ of condition number vs (constant) surface impedance.

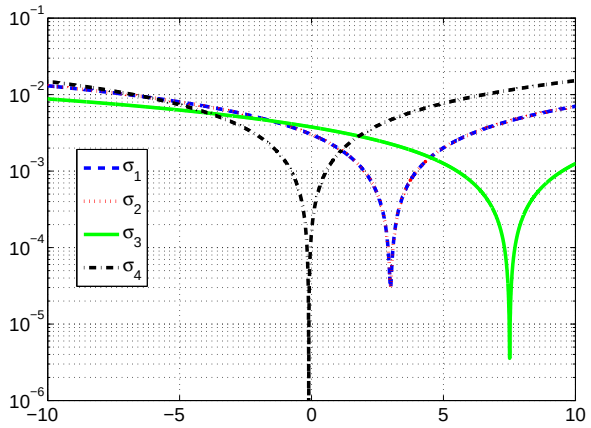

(b) Eigenvalues (absolute value) of the system matrix when $Z_s = jX_s$.

Fig. 3. Square plate - $N_{DoF} = 4$.

is analyzing field jumps across the dielectric interface, and the fields above and below Σ can be correctly reconstructed at the cost of a more expensive Green's function computation. The latter, together with the correct handling of the spatial dispersion in the dielectric slab (key point in guided wave phenomena), indicates that metasurfaces shall be analyzed through the transparent IBC-EFIE of eq. (6).

IV. Numerical Examples

The previous analysis has been carried out for isotropic surface impedances but the results can be applied to the tensorial case. We remark that we have employed our formulation to significant anisotropies (see Sec. IV-B) without problems.

All the numerical results presented in the following sections have been obtained with the formulation of eq. (2); previous sections proved how this is the only formulation capable of handling metasurface problems.

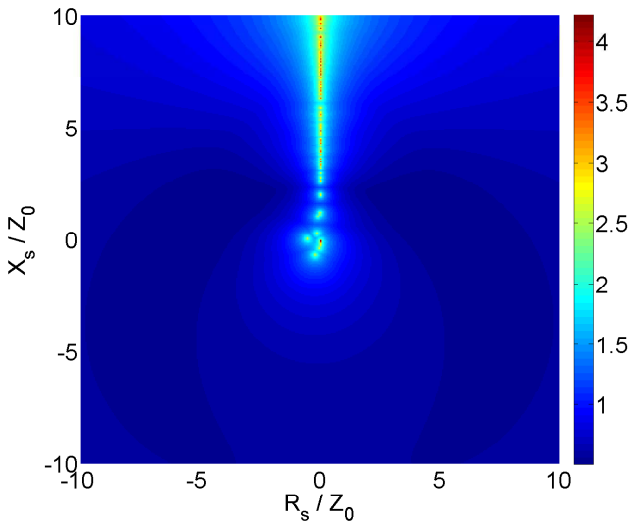

(a) Condition number ($\log_{10}$) of the opaque IBC-EFIE.

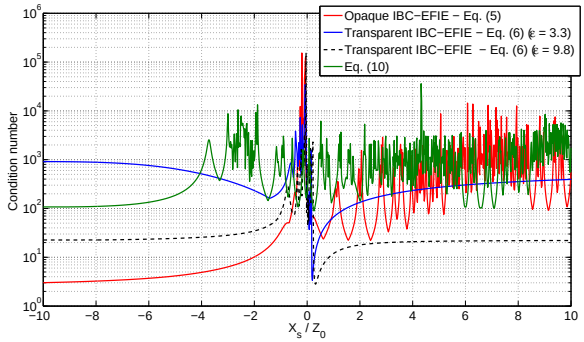

(b) Condition number for imaginary surface impedances - Comparison between different IBC-EFIE formulations.

Fig. 4. Square plate - $N_{DoF} = 313$.

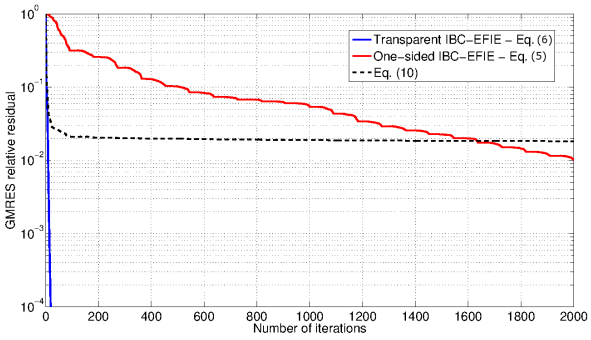

Fig. 5. Convergence of the GMRES solver for the planar Luneburg lens at 7.5 GHz.

A. Isotropic surface impedance: a planar Maxwell's fish-eye lens

In this section, a planar lens implementing the impedance profile of a Maxwell's fish-eye lens is considered:

$$Z_s = jZ_0 \sqrt{\frac{4\left(\frac{k_s}{k}\right)^2}{\left[1+\left(\frac{\rho}{R}\right)^2\right]^2} - 1} \qquad (12)$$

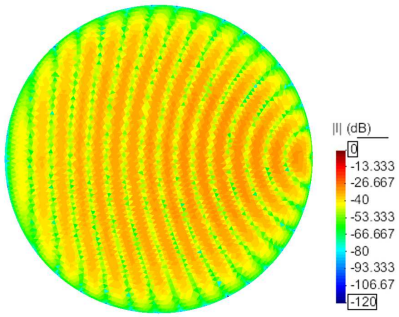

Fig. 6. Surface current density (dBA/m) on the planar Luneburg lens at 7.5 GHz with eq. (6).

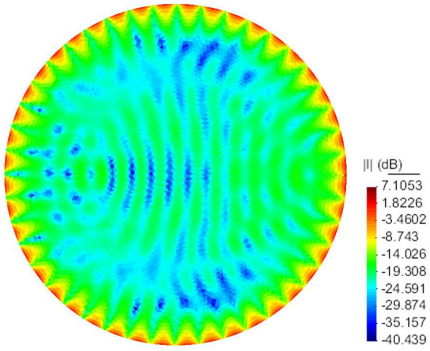

Fig. 7. Surface current density (dBA/m) on the planar Luneburg lens at 7.5 GHz with eq. (5).

where ρ is the distance from the center, $R = 12.5cm$ is the radius of the lens, and k_s is the wavenumber of the TM guided wave supported by the structure (a PEC-backed dielectric slab). The lens has been discretized with 27'866 RWG functions, and analyzed at the frequency of 7.5 GHz. The impedance profile described by (12) possesses the property of focusing each point on its circumference to the point diametrically opposed to it. The lens has been realized on the same substrate of Sec. III-B; it has been excited with a $\hat{z}-$polarized point source located in $(x = 13cm, y = 0)$. Fig. 9 shows the real part of the vertical component of the electric field, on a plane z=5mm (i.e., 3.425mm above the lens): the focusing property of the lens is correctly predicted by the IBC model.

The lens has also been implemented with circular patches with a square slot (possibly null) in the middle, printed on the substrate; the size of the patches and of the slots is varied locally to reproduce the variable impedance profile of eq. (12). The vertical component of the electric field of the actual realization is reported in fig. 10: excellent agreement with the results predicted by the IBC model can be verified (details about the actual realization with patches of the lens can be found in [30]).

B. Anisotropic surface impedance: a beam shifting surface

In this section, a planar beam-shifter based on transformation optics and on the work in [9], is studied through the IBC-EFIE formulation. The beam-shifter is realized with a (constant) anisotropic surface impedance printed on a grounded dielectric slab, as depicted in Fig. 11. The anisotropic region is designed such as to bend by 13° an incident Gaussian beam traveling in the direction $+\hat{x}$ and vertically polarized (along $\hat{z}$), at a frequency of 9 GHz. The beam-shifter is realized with a grounded dielectric slab of thickness $h = 1.55mm$ and permittivity $\varepsilon_r = 14$; on top of the dielectric slab the the anisotropic region has a tensorial reactance, when a Cartesian basis is fixed, described by:

$$[\underline{\underline{Z}}_s] = \begin{bmatrix} jX_{xx} & jX_{xy} \\ jX_{yx} & jX_{yy} \end{bmatrix} \tag{13}$$

with $X_{xx} = -1300\Omega$, $X_{yy} = -1626\Omega$, and $X_{xy} = X_{yx} = 1215\Omega$. Fig. 12 shows the y-component of the magnetic field $H_y = \hat{y} \cdot \mathbf{H}$ on the beam-shifting surface. The Gaussian beam, launched in the isotropic region, excites a surface wave in the grounded slab, which is refracted by 13° when encountering the anisotropic region.

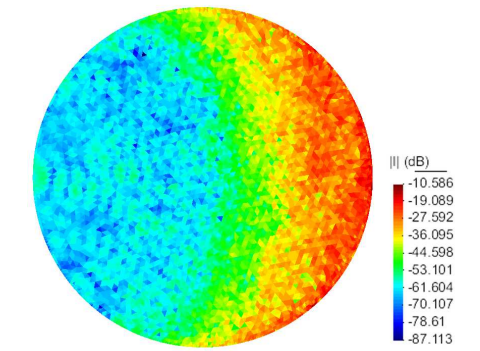

Fig. 8. Surface current density (dBA/m) on the planar Luneburg lens at 7.5 GHz with eq. (10).

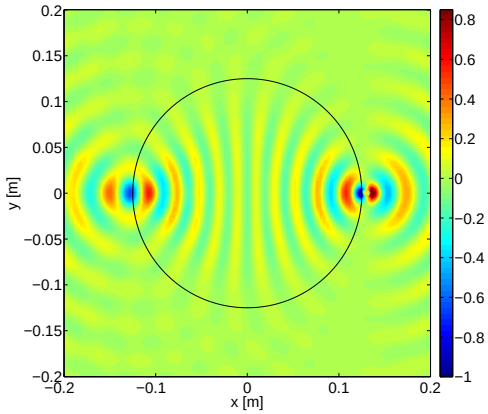

Fig. 9. Planar Maxwell's fish-eye lens: the vertical component (real part) of the electric field (V/m), on a plane 3.425mm above the lens. Results obtained with the IBC model; the circumference delimits the lens region.

C. Anisotropic surface impedance: an holographic antenna

To prove the effectiveness of the approach, we apply it to the analysis of a holographic antenna based on the work in [5]. The antenna is a circular disc with diameter D = 54 cm,

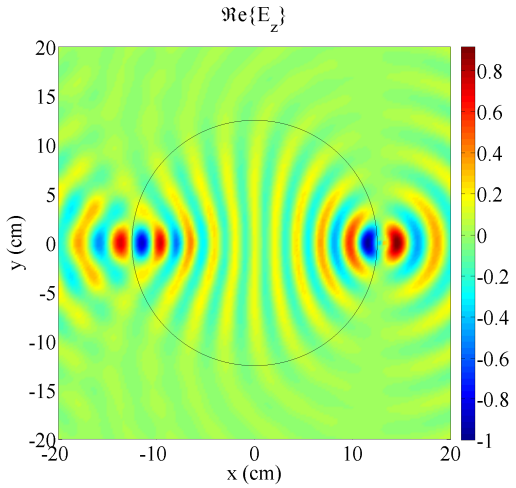

Fig. 10. Planar Maxwell's fish-eye lens: the vertical component (real part) of the electric field (V/m), on a plane 3.425mm above the lens. Results obtained with a full-wave simulation of the actual realization of the lens with patches; the circumference delimits the lens region.

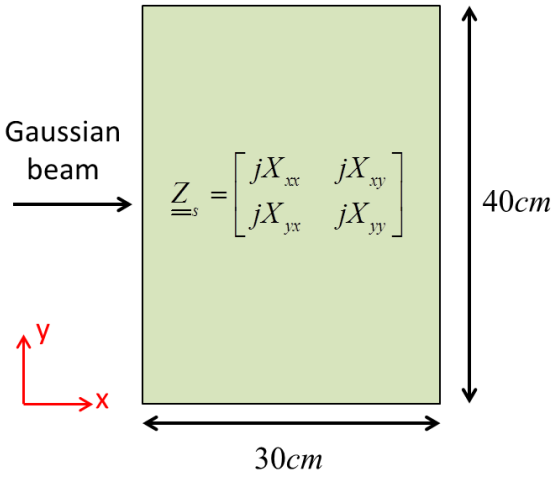

Fig. 11. A beam-shifting surface is realized with a (constant) anisotropic surface impedance printed on a grounded dielectric slab. The anisotropic region is designed to bend an impinging Gaussian incident beam, traveling in the direction $+\hat{x}$ and vertically polarized (along $\hat{z}$), by 13° with respect to the x-axis.

corresponding to about 15 λ at the frequency f_0 = 8.425 GHz, with an anisotropic impedance profile which, fixed the basis in cylindrical coordinates, takes the following form:

$$[\underline{\underline{Z}}_s] = jZ_0 \begin{bmatrix} \eta_{\rho\rho} & \eta_{\rho\phi} \\ \eta_{\phi\rho} & \eta_{\phi\phi} \end{bmatrix} \tag{14}$$

with

$$\begin{aligned} \eta_{\rho\phi} &= \eta_{\phi\rho} = \eta_s\, m\, \cos(K\rho) \\ \eta_{\rho\rho} &= \eta_s \left[1 + m\, \sin(K\rho)\right] \\ \eta_{\phi\phi} &= \eta_s \left[1 - \frac{m}{2}\, \sin(K\rho)\right] \end{aligned} \tag{15}$$

In the above, $\eta_s = 0.55$, $m = 0.3$, $K = 2\pi/d$, and $d = 0.87\lambda = 31mm$ is the radial period of the modulation. The antenna is discretized with 33678 triangular facets, corresponding to 50'079 RWG basis functions, and analyzed with eq. (6) in the

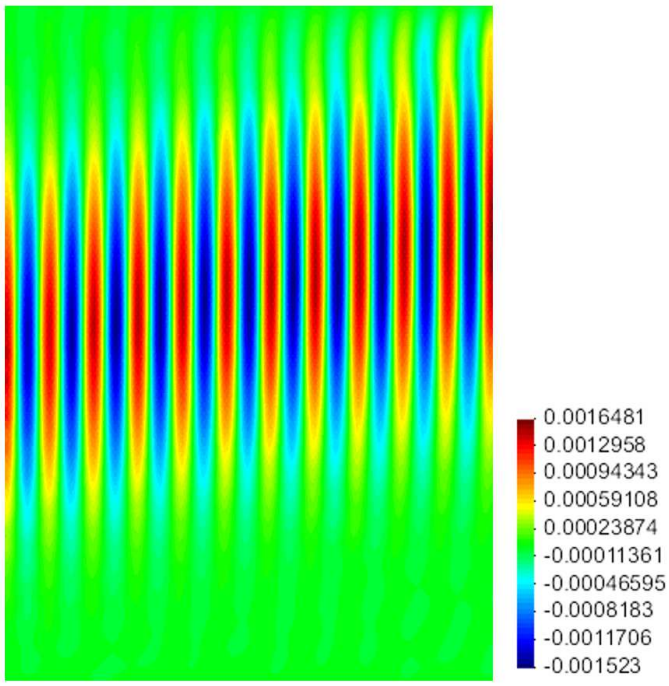

Fig. 12. H_y [A/m]: y-component of the magnetic field on the beam-shifting surface; the incident gaussian beam is bent by 13°.

presence of the Arlon AR 1000 dielectric substrate actually assumed in the rest of the design ($\varepsilon_r = 9.8$, thickness $h = 1.575mm$).

This design has next been implemented with circular patches realizing the reactance of eq. 14 (not reported here), and a simulation of the actual antenna has been carried out, modeling each patch realizing the impedance profile; Fig. 13 shows the comparison between the two models (IBC and actual antenna) for the directivity pattern in the plane $\varphi = 0^\circ$. The excellent agreement between results shows that the IBC model can be considered as a very good approximation of the actual behavior of the metasurface antenna. Its advantages are particularly evident in the design phase, where fast analysis of an impedance surface can be carried out without the need of designing and drawing in the CAD model each patch individually, a process which can be very time consuming, especially when an optimization is required. Note that a variable impedance profile intrinsically requires the single elements to be different from each other (e.g., circular patches with different diameters), even though it is often possible to place them in a periodic (regular) arrangement. It is then clear that an optimization process during design is highly accelerated when only the impedance profile shall be simulated.

It is worth noting that a change in the impedance profile does not require to recompute the system matrix, typically the most time consuming step (especially in the presence of a layered medium, in which Green's functions are non-trivial); it is indeed sufficient to recompute the last term of eq. (6), namely $\hat{\mathbf{n}} \times \left(\underline{\underline{Z}}_s \cdot \mathbf{J} \right)$.

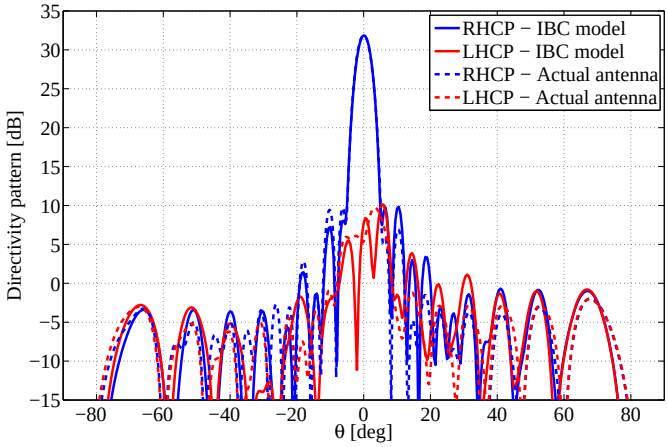

Fig. 13. Directivity pattern of the holographic antenna in a cut in the *xz* plane ($\varphi = 0$); the antenna is fed with a vertical pin, placed in the origin of the reference system (the center of the antenna); RHCP and LHCP refer to, respectively, right hand and left hand circular polarizations.

V. Conclusion

We studied different numerical discretization schemes, based on an integral formulation and on a surface impedance model, for problems involving metasurfaces and guided wave phenomena. Two of the three considered formulations suffer of instability problems in the cases of interest, while the transparent model of the IBC, which only models the thin sheet of patches, yields a stable discretization and accurate results. Results proving the effectiveness of the transparent IBC-EFIE are shown for realistic problems.

Acknowledgment

The authors would like to acknowledge Ingegneria Dei Sistemi (IDS) S.p.A. for having shared the results for the final realization of the Maxwell's fish-eye lens in section IV-A, and of the metasurface antenna in section IV-C. The authors would like to thank D. R. Wilton, University of Houston, TX, for stimulating discussions regarding the subject of this paper.

References

[1] C. L. Holloway, A. Dienstfrey, E. F. Kuester, J. F. OHara, A. K. Azad, and A. J. Taylor, "A discussion on the interpretation and characterization of metafilms/metasurfaces: The two-dimensional equivalent of metamaterials," *Metamaterials*, vol. 3, no. 2, pp. 100 – 112, 2009.

[2] C. Holloway, E. F. Kuester, J. Gordon, J. O'Hara, J. Booth, and D. Smith, "An overview of the theory and applications of metasurfaces: The two-dimensional equivalents of metamaterials," *Antennas and Propagation Magazine, IEEE*, vol. 54, no. 2, pp. 10–35, 2012.

[3] A. M. Patel and A. Grbic, "A printed leaky-wave antenna based on a sinusoidally-modulated reactance surface," *Antennas and Propagation, IEEE Transactions on*, vol. 59, no. 6, pp. 2087–2096, Jun 2011.

[4] G. Minatti, F. Caminita, M. Casaletti, and S. Maci, "Spiral leaky-wave antennas based on modulated surface impedance," *Antennas and Propagation, IEEE Transactions on*, vol. 59, no. 12, pp. 4436–4444, Dec 2011.

[5] G. Minatti, S. Maci, P. De Vita, A. Freni, and M. Sabbadini, "A circularly-polarized isoflux antenna based on anisotropic metasurface," *Antennas and Propagation, IEEE Transactions on*, vol. 60, no. 11, pp. 4998–5009, Nov 2012.

[6] S. Maci, G. Minatti, M. Casaletti, and M. Bosiljevac, "Metasurfing: Addressing waves on impenetrable metasurfaces," *Antennas and Wireless Propagation Letters, IEEE*, vol. 10, pp. 1499–1502, 2011.

[7] M. Bosiljevac, M. Casaletti, F. Caminita, Z. Sipus, and S. Maci, "Non-uniform metasurface luneburg lens antenna design," *Antennas and Propagation, IEEE Transactions on*, vol. 60, no. 9, pp. 4065–4073, Sep 2012.

[8] E. Martini and S. Maci, "Metasurface transformation theory," in *Transformation Electromagnetics and Metamaterials*, D. H. Werner and D.-H. Kwon, Eds. Springer London, 2014, pp. 83–116.

[9] A. M. Patel, "Controlling electromagnetic surface waves with scalar and tensor impedance surfaces," PhD Thesis, University of Michigan, 2013.

[10] S. Yan and J.-M. Jin, "Self-dual integral equations for electromagnetic scattering from IBC objects," *Antennas and Propagation, IEEE Transactions on*, vol. 61, no. 11, pp. 5533–5546, Nov 2013.

[11] E. F. Kuester, M. Mohamed, M. Piket-May, and C. Holloway, "Averaged transition conditions for electromagnetic fields at a metafilm," *Antennas and Propagation, IEEE Transactions on*, vol. 51, no. 10, pp. 2641–2651, Oct 2003.

[12] C. L. Holloway, D. C. Love, E. F. Kuester, J. A. Gordon, and D. A. Hill, "Use of generalized sheet transition conditions to model guided waves on metasurfaces/metafilms," *Antennas and Propagation, IEEE Transactions on*, vol. 60, no. 11, pp. 5173–5186, Nov 2012.

[13] B. Stupfel and D. Poget, "Sufficient uniqueness conditions for the solution of the time harmonic maxwell's equations associated with surface impedance boundary conditions," *J. Comput. Phys.*, vol. 230, no. 12, pp. 4571–4587, Jun 2011.

[14] M. A. Francavilla, E. Martini, F. Vipiana, S. Maci, and G. Vecchi, "Full-wave analysis of tensorial impedance metasurfaces," in *Proceedings of the IEEE Int. Symp. on Antennas and Propagation*, Orlando, FL, 2013, p. 230.

[15] M. A. Francavilla, E. Martini, F. Vipiana, S. Maci, and G. Vecchi, "Numerical simulation of tensorial impedance metasurfaces," in *Proceedings of the 7th European Conference on Antennas and Propagation*, Gothenburg, Sweden, 2013, pp. 3937–3938.

[16] E. Bleszynski, M. Bleszynski, and T. Jaroszewicz, "Surface-integral equations for electromagnetic scattering from impenetrable and penetrable sheets," *Antennas and Propagation Magazine, IEEE*, vol. 35, no. 6, pp. 14–25, Dec 1993.

[17] A. Glisson, M. Orman, F. Falco, and D. Koppel, "Electromagnetic scattering by an arbitrarily shaped surface with an anisotropic impedance boundary condition," *Applied Computational Electromagnetics Society Journal*, vol. 10, no. 3, pp. 93–106, 1995.

[18] K. Achouri, M. A. Salem, and C. Caloz, "General metasurface synthesis based on susceptibility tensors," *arXiv:1408.0273*, August 2014.

[19] B. H. Fong, J. S. Colburn, P. R. Herz, J. J. Ottusch, D. F. Sievenpiper, and J. L. Visher, "Method for designing artificial surface impedance structures characterized by an impedance tensor with complex components," Patent US 7 911 407 B1, 2011.

[20] D. Sievenpiper, "Multiband tunable impedance surface," Patent US 8 212 739 B2, 2012.

[21] J. A. Stratton and L. J. Chu, "Diffraction theory of electromagnetic waves," *Phys. Rev.*, vol. 56, pp. 99–107, Jul 1939.

[22] K. A. Michalski and J. R. Mosig, "Multilayered media green's functions in integral equation formulations," *IEEE Trans. Antennas Propagation*, vol. 45, pp. 508–519, March 1997.

[23] A. M. Patel and A. Grbic, "Modeling and analysis of printed-circuit tensor impedance surfaces," *Antennas and Propagation, IEEE Transactions on*, vol. 61, no. 1, pp. 211–220, Jan 2013.

[24] T. Bertuch, F. Vipiana, and G. Vecchi, "Efficient analysis of printed structures of arbitrary shape on coated cylinders via spatial-domain mixed-potential green's function," *IEEE Transactions on Antennas and Propagation*, vol. 60, no. 3, pp. 1425–1439, 2012.

[25] S. M. Rao, D. R. Wilton, and A. W. Glisson, "Electromagnetic scattering by surfaces of arbitrary shape," *IEEE Trans. Antennas Propagation*, vol. 30, no. 3, pp. 409–418, May 1982.

[26] I. Hanninen and K. Nikoskinen, "Implementation of method of moments for numerical analysis of corrugated surfaces with impedance boundary condition," *Antennas and Propagation, IEEE Transactions on*, vol. 56, no. 1, pp. 278–281, Jan 2008.

[27] L. Medgyesi-Mitschang and J. Putnam, "Integral equation formulations for imperfectly conducting scatterers," *Antennas and Propagation, IEEE Transactions on*, vol. 33, no. 2, pp. 206–214, Feb 1985.

[28] A. M. Patel and A. Grbic, "Effective surface impedance of a printed-circuit tensor impedance surface (PCTIS)," *Microwave Theory and Techniques, IEEE Transactions on*, vol. 61, no. 4, pp. 1403–1413, Apr 2013.

[29] A. M. Patel and A. Grbic, "The effects of spatial dispersion on power flow along a printed-circuit tensor impedance surface," *Antennas and*

Propagation, IEEE Transactions on, vol. 62, no. 3, pp. 1464–1469, Mar 2014.

[30] M. Mencagli, E. Martini, D. Gonzalez-Ovejero, and S. Maci, "Metasurfing by transformation electromagnetics," *Antennas and Wireless Propagation Letters, IEEE*, vol. 13, pp. 1767–1770, 2014.

PLACE PHOTO HERE

Matteo Alessandro Francavilla (M'15) received the Laurea degree in Telecommunication Engineering and Ph.D. degree in applied electromagnetics from Politecnico di Torino, Italy, respectively in 2007 and 2011. During 2007 he spent six months with the Netherlands Organization for Applied Scientific Research (TNO), The Hague, The Netherlands.

During 2010 he carried out part of the Doctoral research as a visiting student at the University of Houston, TX, USA. Since January 2011, he has been working as a researcher at the Antenna and EMC Lab (LACE), at the Istituto Superiore Mario Boella (ISMB), Torino, Italy. His scientific interests include integral equations, numerical techniques for antennas, fast solvers, preconditioners, periodic structures and layered media analysis.

PLACE PHOTO HERE

Enrica Martini (S'98-M'02-SM'13) was born in Spilimbergo (PN), Italy, in 1973. She received the Laurea degree (cum laude) in telecommunication engineering and the Ph.D. degree in informatics and telecommunications from the University of Florence, Florence, Italy, in 1998 and 2002, respectively, and the Ph.D. degree in electronics from the University of Nice-Sophia Antipolis, Nice, France, under joint supervision, in 2002.

She worked at the University of Florence under a one-year research grant from the Alenia Aerospazio Company, Rome, Italy, until 1999. In 2002, she was appointed Research Associate at the University of Siena, Italy. In 2005, she received the Hans Christian Ørsted Postdoctoral Fellowship from the Technical University of Denmark, Lyngby, Denmark, and she joined the Electromagnetic Systems Section of the Ørsted DTU Department until 2007. Since 2007, she has been a Postdoctoral Fellow with the University of Siena, Italy. Since 2012, she has also been with the start-up Wave Up Srl, Florence, Italy. Her research interests include metamaterial characterization, metasurfaces, electromagnetic scattering, antenna measurements, finite element methods, and tropospheric propagation.

PLACE PHOTO HERE

Stefano Maci (M'92-SM'99-F'04) received the Laurea degree (cum laude) in electronics engineering from the University of Florence, Florence, Italy, in 1987.

He is currently Full Professor of Antennas with the University of Siena, Siena, Italy, and Director of the Ph.D. School of Information Engineering and Science, which presently includes about 60 Ph.D. students. His current research interests include high-frequency and beam representation methods, computational electromagnetics, large phased arrays, planar antennas, reflector antennas and feeds, metamaterials and metasurfaces.

Since 2000, he has been a member of the Technical Advisory Board of 11 international conferences and a member of the Review Board of 6 international journals. He has organized 23 special sessions in international conferences and held 10 short courses about metamaterials, antennas, and computational electromagnetics in IEEE Antennas and Propagation Society (AP-S) Symposia. He has been responsible for five projects funded by the European Union (EU). In 20042007 he was WP leader of the Antenna Center of Excellence (ACE, FP6EU) and in 20072010 he was International Coordinator of a 24-institution consortium of a Marie Curie Action (FP6EU). He was the founder of the European School of Antennas (ESoA), a post-graduate school that presently comprises 30 courses on antennas, propagation, electromagnetic theory, and computational electromagnetics, conducted by 150 teachers coming from 15 different countries. He has also been member of the AdCom of the IEEE Antennas and Propagation Society (IEEE AP-S), Associate Editor of the IEEE Transactions on Antennas and Propagation, Chair of the Award Committee of IEEE AP-S, and member of the Board of Directors of the European Association on Antennas and Propagation (EurAAP).

Prof. Maci is presently Director of the ESoA, member of the Technical Advisory Board of the URSI Commission B, member of the Governing Board of the European Science Foundation (ESF) project NewFocus, member of the Italian Committee for Professor Promotion, Distinguished Lecturer of the IEEE Antennas and Propagation Society, member of the Antennas and Propagation Executive Board of the Institution of Engineering and Technology (IET, U.K.). He has been recipient of several awards, among which the EurAAP Carrier Award 2014, and other awards for best papers in conferences and journals. His research activity is documented in 10 book chapters, 120 papers published in international journals (among which 80 on IEEE journals) and about 300 papers in proceedings of international conferences. His h-index is 28, with more than 3000 citations (source Google Scholar).

PLACE PHOTO HERE

Giuseppe Vecchi (M'90-SM'07-F'10) received the Laurea and Ph.D. (Dottorato di Ricerca) degrees in electronic engineering from the Politecnico di Torino, Torino, Italy, in 1985 and 1989, respectively, with doctoral research carried out partly at Polytechnic University (Farmingdale, NY). He was a Visiting Scientist with Polytechnic University in 1989-1990, and since 1990 he is with the Department of Electronics, Politecnico di Torino, where he has been Assistant Professor, Associate Professor (1992 2000), and Professor. He was a Visiting Scientist at the University of Helsinki, Helsinki, Finland, in 1992, and has been an Adjunct Faculty in the Department of Electrical and Computer Engineering, University of Illinois at Chicago, since 1997. His current research activities concern analytical and numerical techniques for analysis, design and diagnostics of antennas and devices, RF plasma heating, electromagnetic compatibility, and imaging.